Chemical Engineering & Processing: Process Intensification 155 (2020) 108057

Contents lists available at ScienceDirect

Chemical Engineering & Processing: Process Intensification

journal homepage: www.elsevier.com/locate/cep

Packed Periodic Open Cellular Structures – an Option for the Intensification of Non-Adiabatic Catalytic Processes

Matteo Ambrosetti[a,b,c], Gianpiero Groppi[a], Wilhelm Schwieger[b,c], Enrico Tronconi[a,**], Hannsjörg Freund[b,c,*]

[a] Politecnico di Milano, Dipartimento di Energia, Via La Masa, 34, 20156 Milano, Italy
[b] Friedrich-Alexander-Universität Erlangen-Nürnberg (FAU), Lehrstuhl für Chemische Reaktionstechnik, Egerlandstraße 3, 91058 Erlangen, Germany
[c] Friedrich-Alexander-Universität Erlangen-Nürnberg (FAU), Anwenderzentrum VerTec, Zentralinstitut für Neue Materialien und Prozesstechnik, Dr.-Mack-Str. 81, 90762 Fürth, Germany

ARTICLE INFO

Keywords:
Process intensification
Additive manufacturing
Structured catalysts
Heat transfer
Pressure drop

ABSTRACT

Conductive structured catalysts offer significant potential for the intensification of gas-solid catalytic processes owing to their enhanced heat transfer properties. A major drawback is the limited catalyst inventory. Recently, packed foams were proposed to overcome the catalyst inventory limitation. The effectiveness of this concept was proven at lab-scale for intensified reactors filled with small catalyst particles. When adopting commercial foams and industrial-scale catalyst pellets, however, poor packing efficiencies are expected, limiting the potential of this concept.

Similarly to foams, Periodic Open Cellular Structures (POCS) grant high heat transfer rates thanks to substantial heat conduction in their solid matrix. Additively manufactured POCS additionally offer great design flexibility. This allows for using a wider range of pellet sizes. In this work, particle packed POCS are introduced and packing efficiencies are systematically studied. Pressure drop in packed POCS is also analyzed and a suitable correlation is proposed. The heat transfer associated with this innovative reactor solution is investigated by performing non-reactive heat transfer experiments. Based on these experiments, a predictive heat transfer model is established and successfully validated with experimental data. The enormous potential of packed POCS for process intensification is illustrated by a case study of a Sabatier pilot reactor.

1. Introduction

Successful design of catalytic reactors should consider the strong coupling between chemical reaction kinetics and transport properties at the micro- and macro-scale. A large portion of catalytic processes is carried out in fixed-bed tubular reactors, where the catalysts in form of granular pellets are randomly loaded inside the tubes. In this configuration, the catalyst inventory is controlled by the pellet shape and the tube-to-particle size ratio. In industrially relevant conditions, the catalyst pellets typically occupy about 60 % of the available reactor volume [1]. Randomly loaded pellets feature point-to-point contacts between each other or with the reactor wall, hampering the static thermal conductivity in both axial and radial direction [2]. In order to provide a sufficient heat transfer for the control of process temperature, avoid undesired losses of activity and selectivity as well as unsafe operation, the convective heat transfer mechanism should be boosted by operating the systems at high specific mass flow rates [3]. These requirements from the heat transfer directly impact on the pressure drop and the reactor design since very long tubes are needed to reach significant conversion in kinetically limited processes. In some cases, catalyst pellets are diluted with chemically inert, thermally conductive particles, thus reducing the local thermal load by deliberately decreasing the active phase inventory [4,5].

In the last decades, structured reactors have been proposed as a potential solution for process intensification thanks to the possibility of tailoring the transport properties of the catalytic reactor [6]. To this end, different internals were investigated in view of their enhanced heat transfer properties [7,8]. One of the possible approaches towards process intensification is the adoption of structures that aim at increasing the convective heat transfer rates such as, for example, static mixers or

* Corresponding author at: Friedrich-Alexander-Universität Erlangen-Nürnberg (FAU), Lehrstuhl für Chemische Reaktionstechnik, Egerlandstraße 3, 91058 Erlangen, Germany.
** Corresponding author at: Politecnico di Milano, Dipartimento di Energia, Via La Masa 34, 20156 Milano, Italy.
E-mail addresses: enrico.tronconi@polimi.it (E. Tronconi), hannsjoerg.freund@fau.de (H. Freund).

https://doi.org/10.1016/j.cep.2020.108057
Received 3 April 2020; Received in revised form 6 July 2020; Accepted 16 July 2020
Available online 19 July 2020

Nomenclature

Latin letters

CI	Catalyst inventory [kg/m^3]
CPI	Cells per inch [m^{-1}] d_{cell} = 0.0254/CPI
c_p	Gas heat capacity [J kg^{-1} K^{-1}]
d_{cell}	POCS cell diameter [m]
d_{pellet}	Pellet diameter [m]
d_s	POCS strut diameter [m]
d_{window}	POCS window diameter [m]
d_t	Tube diameter [m]
G	Specific mass flow rate [kg m^{-2} s^{-1}]
$h_{w,packing}$	Packing wall heat transfer coefficient [W m^{-2} K^{-1}]
$h_{w,POCS}$	POCS wall heat transfer coefficient [W m^{-2} K^{-1}]
$h_{w,oil,wall}$	Oil wall heat transfer coefficient [W m^{-2} K^{-1}]
k_{gas}	Gas thermal conductivity [W m^{-1} K^{-1}]
k_{pellet}	Pellet thermal conductivity [W m^{-1} K^{-1}]
$k_{solid,POCS}$	POCS bulk thermal conductivity [W m^{-1} K^{-1}]
$k_{eff,Packing}$	Packing effective thermal conductivity [W m^{-1} K^{-1}]
$k_{eff,POCS}$	POCS effective thermal conductivity [W m^{-1} K^{-1}]
Nu	Nusselt number [-] Nu = $h_{w,POCS}$*k_{gas}/d_{cell}
Pe_{rif}	Radial Peclet number in packed bed reactors [-]
Pr	Prandtl number [-]Pr = μ c_p / k_{gas}
Re	Reynolds number [-] Re = G d_{pellet}/ μ
Q	Volumetric flow rate [m^3 s^{-1}]
R	Ratio between POCS window diameter and pellet diameter [-]
R_{IF}	Heat transfer resistance between packing and POCS [K m^2 W^{-1}]
R_{INT}	Concentrated internal heat transfer resistance [K m^2 W^{-1}]
R_P	Internal heat transfer resistance of the packing [K m^2 W^{-1}]
R_{POCS}	Internal heat transfer resistance of the POCS structure [K m^2 W^{-1}]
R_{wall}	Concentrated heat transfer resistance at the wall [K m^2 W^{-1}]
r	Radial coordinate [m]
$S_{v,Packing}$	Specific surface area of the pellets in packed POCS system [m^{-1}]
$S_{v,POCS}$	Specific surface area of POCS [m^{-1}]
$S_{v,Tot}$	Specific wetted surface area [m^{-1}]
T	Temperature [K]
T_c	Mean-cup Temperature [K]
T_{wall}	Wall temperature [K]
U	Apparent heat transfer coefficient [W m^{-2} K^{-1}]
$U_{overall}$	Overall heat transfer coefficient [W m^{-2} K^{-1}]
$U_{POCS-Packing}$	Heat transfer coefficient between POCS and packing [W m^{-2} K^{-1}]
u	Gas velocity [m s^{-1}]
$V_{pellets}$	Volume of the pellets [m^3]
V_{POCS}	Volume of the solid of the POCS structure [m^3]
V_{total}	Volume of the sample [m^3]
z	Axial coordinate [m]

Greek letters

ΔP/L	Pressure drop per unit length [Pa m^{-1}]
$\varepsilon_{Packing}$	Porosity of the packing pattern [-]
ε_{PB}	Porosity of a packed bed [-]
ε_{POCS}	Porosity of the POCS [-]
ε_{tot}	Total porosity [-]
μ	Gas viscosity [Pa s]
ρ_{Cat}	Catalyst density [kg/m^3]
ρ_{gas}	Gas density [kg/m^3]

fluid guiding vanes [9–11].

Heat transfer in conductive honeycombs was studied experimentally in both non-reactive and reactive tests [12], showing high effective thermal conductivities and very high overall heat transfer rates, limited by the coupling between the reactor tube wall and the monolith structure. The successful application of washcoated aluminum monoliths for the oxidation of o-xylene to phthalic anhydride in a pilot-scale industrial tubular cooled reactor is reported in [13]. Micro-channel metallic reactors [14] have been proposed as an alternative solution to intensify different catalytic processes thanks to their enhanced thermal conductivity and the increase of the volumetric heat exchange area. These structured reactors have been applied at the lab-scale for the intensification of the Fischer-Tropsch synthesis [15], steam methane reforming [16], methanol dehydration, ammonia oxidation and the water-gas-shift reaction [17].

Open cell foams are disordered cellular materials characterized by an interconnected solid matrix with permeable pores. Similarly to honeycombs, they may grant high static heat conduction in their interconnected matrix and are therefore considered as potential advanced catalyst supports [18]. Applications of open cell foams to several catalytic processes have been reported in literature (e.g. methanol synthesis [19], steam reforming [20], Fischer-Tropsch synthesis [21], catalytic partial oxidations [22], CO_2 methanation [23]). Recently, so-called Periodic Open Cellular Structures (POCS) have been proposed as innovative catalyst supports by some of us [24]. These structures retain all the advantageous features associated with open cell foams such as high surface area, permeability in all directions and an interconnected solid structure. In addition, their ordered design combined with Computer Aided Design techniques and modern additive manufacturing methods (3D printing) allows for optimizing their geometry towards the process needs, thereby increasing the heat conduction with respect to foams thanks to uniform strut shapes [25,26] and thus offering additional degrees of freedom in the design of catalytic reactors [4,27]. Applications of 3D printed catalyst supports have been recently reported for the process intensification of NO oxidation [27] and for COx methanation [7,8].

One of the major drawbacks of structured catalysts is the limited catalyst inventory allowed by the current activation methodologies, which are mainly based on washcoating. With spin-coating, dip-coating or electrodeposition it is possible to load at most 20 % of the reactor volume with a catalyst – in contrast to the volumetric loadings in excess of 60 % that can be reached in packed bed reactors using bulk catalyst particles [3]. Moreover, coating of these structures can be more challenging than coating of pellets with respect to the mechanical stability of the coating layer as well as the accessibility of the inner parts of the structure. This is a relevant issue also for processes where catalyst inventory is not a key bottleneck because very active formulations are available and egg-shell solutions are typically adopted to maximise the active phase efficiency.

In order to exploit the advantages associated with structured catalysts [6] while avoiding problems related to the coating deposition, it was proposed to pack the cavities of structured reactors with catalyst pellets according to the concept of the three level of porosity reactor [28]. Along these lines, a research group from TU Delft first proposed the configuration of packed cross flow structures [29,30]. In these systems, a boost of the heat transfer mechanism can be achieved by a smart design of the structures that allows the optimal distribution of gaseous and liquid phases. The concept of packed structures was later extended to packed metallic monoliths [31]. More recently, some of us demonstrated that also the complex structure of open cell foams can be

effectively packed with small catalyst particles, provided that the particle size is sufficiently smaller than the foam pores [3]. Studies of packed foams under non-reactive conditions showed that the heat transfer mechanisms of packed pellets and foams act in synergy. At the tube wall, the packed bed ensures the coupling with the wall and provides an efficient heat transfer. The continuous solid matrix of the foam features a high effective radial thermal conductivity over the whole cross section of the reactor, close to that of unpacked open cell foams. The increased heat transfer rates associated with the presence of conductive internals and the adoption of small particles that can fit into the cavities of the structures enable the design of compact reactors with highly active catalysts. The concept was then applied to Fischer-Tropsch synthesis [32] and steam reforming [33,34] with the aim of designing a compact gas-to-liquid process able to exploit remote gas feedstock. In comparison to conventional packed bed reactors, at low flow rates the advantages of the packed foam system both in the case of a strongly exothermic catalytic reaction (e.g. Fischer-Tropsch) and in the case of an equilibrium limited endothermic reaction (e.g. Methane Steam Reforming) were remarkable in terms of conversion and shape of the temperature profiles. In the case of Fischer-Tropsch synthesis, 300 μm pellets were fitted into the cavities of commercial Al foams in order to cope with the stringent intraparticle diffusion limitations associated with the liquid waxes filling the catalyst pores. A different strategy was adopted in the case of methane steam reforming based on the use of egg-shell particles which maximize the Rh catalyst effectiveness. However, still relatively small 600 μm pellets were adopted to obtain a high packing efficiency enabling a reasonable catalyst inventory in commercial foams.

In a recent work [35], the packing efficiency of open cell foams was shown in fact to be a function of the foam pore window-to-pellet diameter ratio, dropping down for values of the ratio lower than 1.5. Accordingly, since the largest commercially available pore window size is close to 2.5 − 3 mm, open cell foams can be packed only with pellets smaller than 2 mm. This is a clear limitation of the concept since many industrial catalytic processes make use of pellets much larger than 2 mm, therefore the application of packed foams in those processes is not feasible [36] unless a change in the pellet design is allowed.

In this regard, the advantages associated with the flexible and well-defined design of POCS may help in partially overcoming this limitation while at the same time enabling enhanced heat transfer rates in thermally limited catalytic processes. Therefore, in this work the concept of particle packed POCS as shown in Fig. 1 is introduced and explored in a systematic manner.

We systematically investigate the packing efficiency of POCS as function of the window-to-pellet size ratio. This helps to identify the limits of operation and to derive a correlation that can be used for the design of the supports in function of the targeted catalyst density. We also determine experimentally the pressure drop of packed POCS for different combinations of cell shapes, cell sizes and pellet diameters to assess and compare the performance of the proposed solution with that of conventional packed beds. An engineering correlation, derived as an extension of the well-known Ergun equation, is also proposed for the estimation of pressure drop inside packed POCS in analogy to packed foams. Finally, experimental tests dedicated to the systematic study of heat transfer in these systems are performed in a wall-jacketed tubular reactor and heat transfer coefficients for each test are estimated from the collected temperature profiles by means of mathematical modelling. The effects of cell size, bulk thermal conductivity of the material, pellet size and mass flow rates on the overall heat transfer rates are investigated. A heat transfer model is developed by considering all the possible heat transport pathways and computing the thermal resistances associated with the different elements of the electrically equivalent circuit according to previously derived engineering correlations.

Finally, we use the derived correlations to perform a comparative study of the advantages of packed POCS in terms of overall heat transfer rates and pressure drop under industrially relevant conditions. The solution provides a remarkable advantage in terms of heat transfer without detrimental effects on pressure drop for a wide range of flow rates characteristic of industrial scale reactors or intensified applications.

2. Experimental methods

2.1. Investigated POCS samples

In this work, several POCS samples with different unit cell types (cubic, diamond, tetrakaidecahedron -TKKD), cell sizes and porosities were manufactured in order to perform experimental tests with regard to the packing efficiency, pressure drop and heat transfer. POCS were designed with the CAD software OpenSCAD by repeating the respective unit cell in all spatial dimensions. Besides the definition of the respective unit cell type, the further design parameters of the structures were the cell size and the strut diameter. The different unit cell types are shown in Fig. 2.

The porosity was calculated and verified a posteriori. The other geometrical properties of the different structures were quantified using the models proposed by Klumpp et al. [37] (Eq. (1)) for ideal cubic cells and by Lämmermann et al. [38] for diamond and TKKD unit cells, respectively (Eqs. (2) and (3)).

$$\text{Cubic cell} \quad d_{window} = d_{cell} - d_s \tag{1}$$

$$\text{Diamond cell} \quad d_{window} = \left(\frac{6\sqrt{3}}{\pi}\right)^{0.5}\left(d_{cell}\frac{\sqrt{3}}{4} - \frac{\sqrt{3}}{3}d_s\right) \tag{2}$$

$$\text{TKKD cell} \quad d_{window} = \left(\frac{6\sqrt{3}}{\pi}\right)^{0.5}\left(d_{cell}\frac{\sqrt{2}}{4} - \frac{\sqrt{3}}{3}d_s\right) \tag{3}$$

The diameter of the POCS samples was dimensioned in order to tightly fit either into the 30 mm I.D. PVC tube of the cold-flow setup used for pressure drop measurements or the 25 mm I.D stainless steel tube used for heat transfer runs. The length of the samples used for the pressure drop tests was chosen such that only samples longer than at least five times the cell size were used and only pressure drop

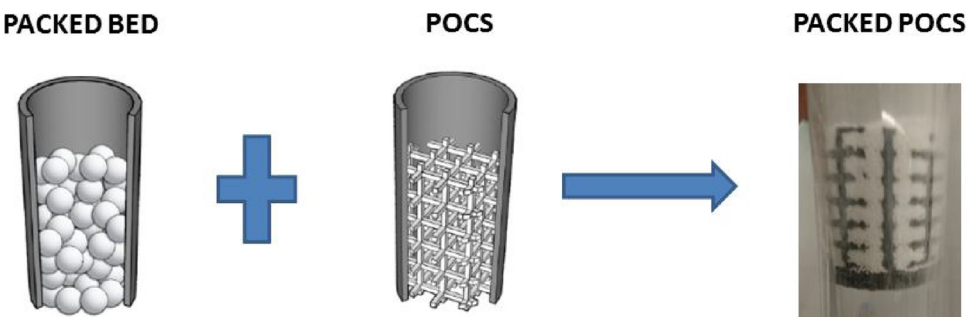

Fig. 1. The concept of packed POCS.

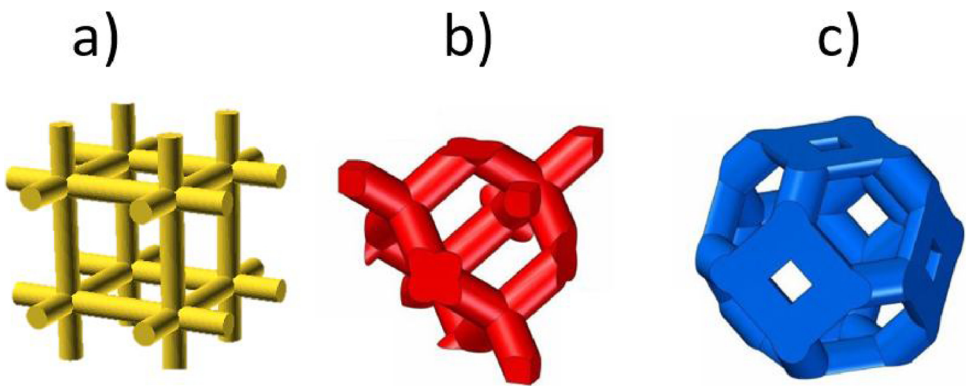

Fig. 2. Unit cells of POCS used in this work: a) cubic cell, b) diamond cell, c) tetrakaidecahedron cell.

measurements higher than 10 mbar were considered.

Samples for pressure drop tests (see Table 1) were printed in ABS (Acrylonitrile Butadiene Styrene polymer) with a Fused Deposition Modelling (FDM) 3D Printer Ultimaker 2+ with a nozzle of 0.2 mm. In an optimized printing procedure, the nozzle was kept at 250 °C and the building plate was kept at 95 °C. In order to ensure adequate 3D printing resolution, only structures characterized by struts bigger than 0.5 mm (2.5 times the nozzle diameter) were considered in the experimental campaign.

Samples for heat transfer tests (see Table 2) were additively manufactured in Ti6Al4V and in AlSi10Mg to assess the effect of the bulk material thermal conductivity and geometries on the overall heat transfer performance. The POCS made of Ti6Al4V were produced by selective electron beam melting (SEBM) whereas the POCS in AlSi10Mg was manufactured by selective laser melting (SLM). More details about these manufacturing methods are provided in [4,39]. As reported by Busse et al. [4], the 3D printing techniques adopted for the manufacturing of the samples used in this work (FDM and SEBM) produce samples with equal total and hydraulic porosity (i.e., no hollow struts).

2.2. Packing density measurements

For the packing tests, both metallic and polymeric structures were employed and we proved that the packing density is a function of the pellet and of the POCS geometry only, thus being independent of the POCS material.

Packing densities for different combinations of pellets/structures were evaluated by weighing the amount of material that was loaded inside the cavities of the structure. Commercial spherical glass beads from Sigma Aldrich and γ-Al_2O_3 spherical pellets from Sasol as given in Table 3 were used in the experimental studies. The particle size and density of the bulk pellets were evaluated as described in [35].

The packing density of beds with large tube-to-particle diameter ratio was computed by weighing the mass of loaded particles and evaluating the void fraction. In the case of the non-porous glass beads, we also evaluated the void fraction by adding water into the cavities of the bed in a control volume. As expected, asymptotic bed porosities of 0.38 were observed [35].

These packing tests were aimed at determining the packing density ($1-\varepsilon_{Packing}$) in the empty spaces of the POCS structure. The packing efficiency is evaluated as follows [35]:

$$1 - \varepsilon_{Packing} = \frac{V_{pellets}}{V_{total} - V_{POCS}} = \frac{V_{pellets}}{\varepsilon_{POCS} V_{total}} \quad (4)$$

To enhance the density of the packing, the external part of the sample holder was set into mechanical vibration. The reproducibility of these measurements was carefully monitored, particularly in the case of small window-to-particle diameter ratios.

Table 1
Morphological properties of POCS used for pressure drop tests.

Cell shape	Cells per inch (CPI)	ε_{POCS} [-]	d_{window} [mm]	d_{strut} [mm]	S_v [m^{-1}]
Cubic	3	0.902	7.00	1.5	165
Diamond	3	0.812	4.57	2	411
TKKD	3	0.777	3.34	2	450
Diamond	4	0.896	3.95	1	423
TKKD	4	0.856	3.03	1	487
Cubic	5	0.774	3.08	2	471
Cubic	6	0.890	3.23	1	414
Diamond	6	0.836	2.39	0.9	775

2.3. Experimental measurements of the pressure drop

Pressure drop measurements were performed in a cold-flow setup (see Fig. 3) comprising a PVC tube with an inner diameter of 30 mm. The air flow rate was regulated with a mass flow controller (MASSSTREAM™ D-6361, scale: 4-200 NLM[1]) in the range from 5 to 120 NLM and fed to the tube at ambient temperature. For the loading procedure, a thin disk of a commercial foam (60 PPI NiFeCrAlloy provided by Alantum GmbH, $\varepsilon = 0.9$, thickness 3 mm) was placed in between the two pressure ports, and then the POCS sample was tightly fitted inside the tube by means of a plug. Then, the particles were poured from the top of the tube, entering the void space and thereby forming a packed structure. Finally, a second foam disk was stacked to confine the particles. Packing densities were calculated from the weight of the loaded material. A differential manometer Testo 410 with a full scale of 100 mbar and a sensitivity of 0.1 mbar was connected with flexible PVC tubes to the pressure ports and used for all the performed experimental tests.

The pressure drop of the foam disks was measured individually, and negligible values (< 1 %) with respect to the pressure drop of the packed bed and the packed POCS were recorded. The reason for this is the fact that the porosity of the foam is much higher than that of the packed bed or the packed POCS, respectively.

2.4. Heat transfer experiments

The heat transfer performance of packed POCS was evaluated by running non-reactive heat transfer experiments under steady state conditions using the setup displayed in Fig. 4 and described in [4].

Air was fed to the test tube by means of the same mass flow controller used for the pressure drop tests. For the heat transfer runs, the influence of the flow rate was investigated in the range from 5 to 100 NLM. The test tube consists of three modular parts (inlet section, heated

[1] 1 bar and 273.15 K

Table 2
Morphological properties of POCS used for heat transfer tests.

Cell shape	CPI	ε_{POCS} [-]	d_{window} [mm]	d_{strut} [mm]	S_v [m^{-1}]	Material	Bulk Thermal conductivity [W/m/K]
Cubic	5	0.94	4.78	1.03	428	Ti6Al4V	6.7
Cubic	7	0.86	3.39	1.08	772	Ti6Al4V	6.7
Cubic	9	0.90	2.72	0.77	770	Ti6Al4V	6.7
Cubic	5	0.92	4.97	0.99	398	AlSi10Mg	150

Table 3
Geometrical properties of pellets used for packing tests.

Material	d_{pellet} nominal [mm]	ρ_{pellet} [g/cm^3]	d_{pellet} average [mm]	d_{tube} / d_{pellet} [-]
Al_2O_3	0.6	1.14	0.64	46.9
Al_2O_3	0.8	1.11	0.92	32.6
Al_2O_3	1	1.23	1.04	28.9
Al_2O_3	1.2	1.08	1.18	25.4
Al_2O_3	1.6	1.08	1.70	17.6
Glass	0.5	2.45	0.56	53.6
Glass	1	2.45	1.13	26.5
Glass	2	2.11	1.83	16.4

tube, outlet section) connected with DK-25 vacuum flanges. The inlet and the outlet were kept at ambient temperature, whereas the mid-section was heated by means of the external jacket. Sealings between cold and hot parts of the setup were made of customized PEEK flanges in order to host two grooves for silicon O-rings.

In the inlet section, a diamond unit cell type structure was used as static mixer for homogenization of the air flow field. At the outlet of the heat exchanger, a tube fitted with a static mixer was installed. The static mixer at the outlet of the reactor was modified in order to host temperature probes. Three multipoint thermocouples of type K (diameter equal to 1.5 mm, sampling points with 30 mm distance between each other) were used in the experimental campaigns. Axial temperature profiles at the centerline as well as at two further radial positions of 5 mm and 10 mm from the centerline were recorded by axially sliding the multipoint thermocouples with a sampling interval of 1 cm. The structures investigated in this work were of 10 cm length, therefore 11 axial measurements were taken for each temperature profile. As in the case of pressure drop, high cell density foam disks were placed at the inlet and at the outlet of the investigated system to keep the particles in the system. The foam disk towards the outlet of the reactor was modified to allow the passage of the thermocouples. The temperature values were recorded with a data logger PCE-T 1200.

The shell side of the heat exchanger consisted of a DN-50-KF flange forming an annular heating jacket (ID = 29 mm, OD = 45 mm) connected to the inlet and to the outlet of the thermo oil circuit.

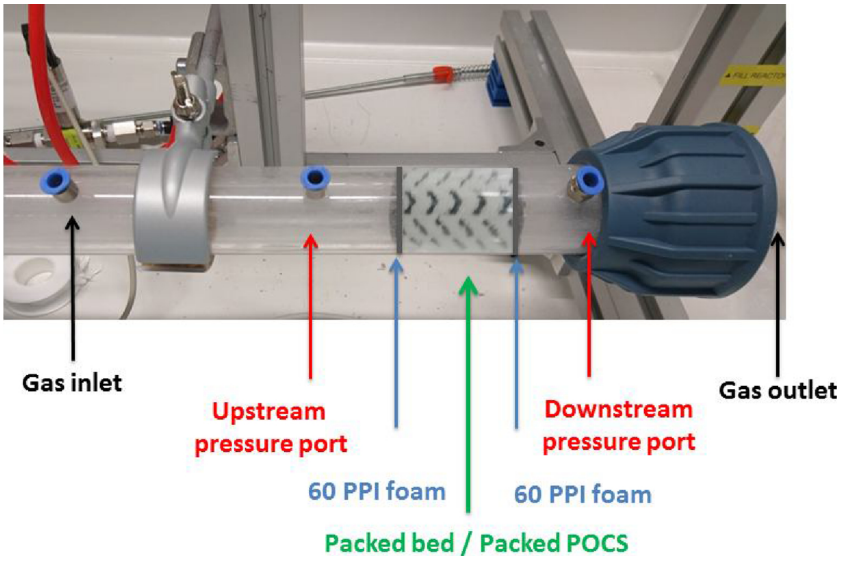

Fig. 3. Experimental setup used for the pressure drop measurements.

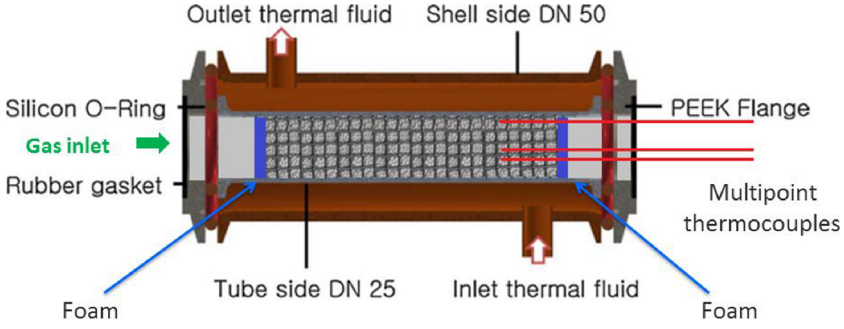

Fig. 4. Layout of the test tube used for the heat transfer measurements.

Marlotherm™ was used as heat transfer fluid and was heated and fed to the rig by means of a thermostat Huber model CC-202C with a flow rate of 10 L/min. The temperature of the thermal fluid was measured at the inlet and outlet of the shell with 2 K-type thermocouples. Temperature differences less than two degrees were recorded between inlet and outlet of the test tube. For the quantification of the heat transfer coefficients, the average temperature was considered as constant along the whole axial profile.

3. Results and discussions

3.1. Evaluation of the packing density in packed POCS

About 30 combinations of pellets and POCS samples were tested for the evaluation of the packing density according to Eq. 4. Results are shown in Fig. 5 by plotting the measured packing porosity against the ratio of the window size of the structure to the particle diameter.

$$R = \frac{d_{window}}{d_{pellet}} \tag{5}$$

The trends in Fig. 5 are similar to those reported for packed foams [35]. For large R (≥5), the porosity data are almost superimposed to the asymptotic porosity in packed bed reactors (i.e. 0.38). The packing porosity increases with the decrease of R. At R approaching a value of unity, the porosity drastically increases. The ratio R = 1 represents in fact a physical limit since the particles would have the same size of the windows and, therefore, they cannot be packed into the structure. As observed with foams, in a narrow range of R the porosity increases from values around 0.45 at R = 3 to 0.65 at R = 1.5. For R less than 1.5, the packing is extremely loose and irregular, with evidence of partially unfilled cavities inside the structure [35]. This may represent a problem in practical applications since such cavities offer preferential flow paths inside the reactor which can lead to pronounced bypass effects and uneven velocity and temperature distributions. Accordingly, we did not perform any measurements under these conditions. It is worth noticing that, with the adoption of the window-to-particle diameter ratio as the relevant parameter for packing density, it is possible to reconcile the collected data. On the other hand, at large values of R the porosity approaches the asymptotic value of a packed bed with large tube-to-particle diameter ratio, consistently with the experimental conditions herein investigated (Table 3).

To describe the observed behavior, a correlation was derived based on a literature one for classical packed bed reactors [1]. This literature correlation proposed by Dixon estimates the porosity in packed bed reactors with spherical particles as an asymptotic contribution and additional terms which depend on the tube-to-particle diameter ratio. In packed POCS, we here replace this quantity by the window-to-particle size ratio. From Fig. 5 it is evident that for large window-to-particle size ratios, the void fraction converges to the asymptotic value of a packed bed. On the other hand, we constrained the parameters of the correlation to satisfy the physical limit for R = 1. Performing a numerical regression, the correlation given in Eq. (9) was derived:

$$\varepsilon_{Packing} = 0.375 + A\left(\frac{d_{pellet}}{d_{window}}\right) + B\left(\frac{d_{pellet}}{d_{window}}\right)^2 \tag{6}$$

$$\lim_{(d_{window}/d_{pellet})\to\infty} \varepsilon_{Packing} = 0.375 \tag{7}$$

$$\lim_{(d_{window}/d_{pellet})\to 1} \varepsilon_{Packing} = 1 \tag{8}$$

$$\varepsilon_{Packing} = 0.375 + 0.018\left(\frac{d_{pellet}}{d_{window}}\right) + 0.607\left(\frac{d_{pellet}}{d_{window}}\right)^2 \tag{9}$$

It is worth mentioning that the proposed correlation is valid for ratios of $d_{tube}/d_{pellet} > 10$, otherwise the asymptotic term in Eq. (9) – 0.375 - should be replaced by the corresponding void fraction of the packed bed, which can be estimated with, e.g., the correlation of Dixon [1]. This may be relevant when packed POCS are applied to systems characterized by small tube-to-pellet ratios.

This correlation fits the experimental data very well, with a maximum deviation of 2 % and a mean error equal to 0.7 %. Accordingly, it can be used to predict the catalyst inventory for different combinations of particle and POCS geometries with a high confidence level.

As an example, Fig. 6 A) displays computed packing porosities for pellet sizes in the range of 0.3 − 3 mm and different POCS samples characterized by a cell size of 5 mm and of different porosities. Fig. 6 B) shows the catalyst inventory that can be loaded in a reactor filled with different POCS by using catalyst pellets with a density of 1000 kg/m^3.

At fixed cell size and porosity, POCS based on a cubic unit cell contain a larger fraction of particles compared to the other (unit cell) structures thanks to the larger window diameter that facilitates the packing. Structures characterized by a low void fraction exhibit lower packing efficiency, owing to the larger struts and higher surface area that adversely interact with the particles. Fig. 6 A) and B) can be used to understand the impact of the structural geometrical properties on the packing efficiency. The actual catalyst load per unit volume (CI) can be computed from the catalyst density, packing density and the structure porosity as follows:

$$CI_{packed\ Pocs} = \rho_{Cat}\,\varepsilon_{POCS}\,(1 - \varepsilon_{Packing}) \tag{10}$$

Moreover, from Fig. 6 B) it can be seen how the different combinations of pellets and structures lead to a different catalyst inventory. As suggested by Eq. (10), the catalyst inventory is directly dependent on the POCS void fraction. For small pellet diameters, the catalyst inventory is only influenced by the porosity of the structure. With increasing pellet size, the catalyst inventory reduction additionally depends on the ratio of the pore/pellet diameters. Typical values for packed beds and washcoated structures are also given as reference for a catalyst density equal to 1000 kg/m^3.

For the same value of the packing porosity, the lower the porosity of the structure, the lower the material load that can be achieved in the reactor. With this solution, a larger reactor volume is required in order to pack the same amount of catalyst, which implies adopting either longer or bigger tubes. The choice may depend on other process characteristics (especially pressure drop or heat transfer limitations).

3.2. Pressure drop in packed POCS

At first, for orientation and validation of the experimental setup measurements of pressure drop in a packed bed were performed, and the results were compared to an Ergun-type correlation [40]. Several measurements were then performed for the assessment of pressure drop

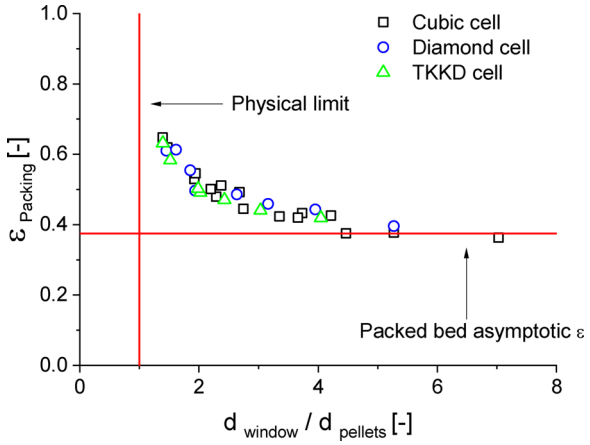

Fig. 5. Packing efficiency for different structures in function of the window-to-pellet diameter ratio.

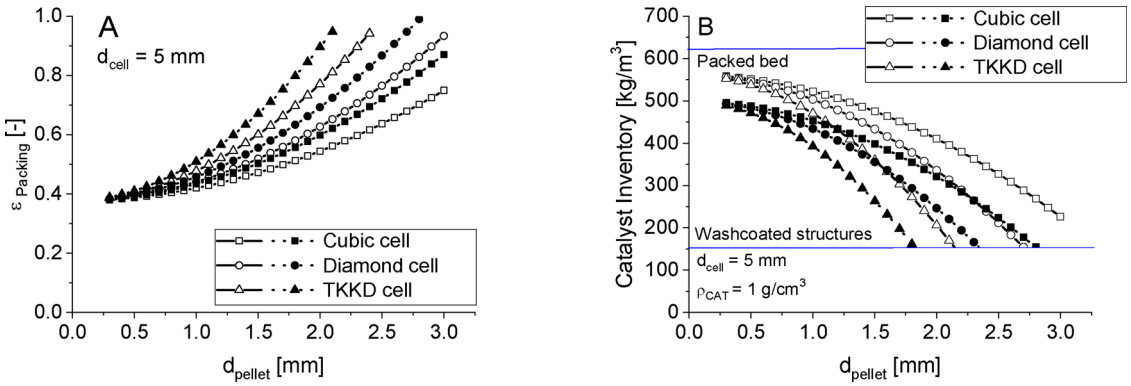

Fig. 6. Packing efficiencies (A) and catalyst inventory (B) for different POCS samples with a cell size equal to 5 mm in function of the pellet diameter: open symbols structures with $\varepsilon_{POCS} = 0.9$, full symbols $\varepsilon_{POCS} = 0.8$; mean values for washcoated structures and packed bed are plotted as reference.

in packed POCS systems. The pressure drop measured at different gas velocities in three POCS packed with particles are compared in Fig. 7 to those measured in a packed bed made of the same material (Al_2O_3 particles with d_{pellet}600 μm).

The pressure drop of bare POCS is much lower than that of packed bed reactors, as documented in [38], due to differences in porosity, surface area and the flow field. The packed POCS instead feature a porosity that is similar to packed bed reactors thanks to the presence of the particles, therefore, a comparison between these systems may be performed.

In Fig. 7 it can be noticed that, despite the presence of the POCS inside the reactor, the pressure drop is typically lower than for conventional packed beds. This is because the total porosity ε_{tot} of the packed structured systems is higher than in conventional packed beds. In fact, as shown by Eq. (11), the total porosity can be evaluated as the product of the porosity of the POCS ε_{POCS} times the porosity of the packed particle evaluated as the complement to the packing efficiency defined by Eq. (4). The decrease of the packing efficiency with low d_{window}/d_{pellet} ratio is responsible for the relatively high porosity of the two 6 CPI structures reported in Fig. 7.

$$\varepsilon_{tot} = \frac{V_{void}}{V_{total}} = \frac{V_{void}}{(V_{total} - V_{POCS})} \frac{(V_{total} - V_{POCS})}{V_{total}} = \varepsilon_{Packing}\varepsilon_{POCS} \tag{11}$$

The 3CPI structure, in contrast, features a lower porosity compared to a conventional packed bed, but still results in a lower pressure drop. The reason for this behavior is probably due to a reduction of the wetted surface area.

A widely recognized correlation for calculating the pressure drop in packed beds was proposed by Ergun and Orning [41]. The Ergun equation can be written in the form:

$$\frac{\Delta P}{L} = 4.17\frac{(S_v)^2}{\varepsilon_{tot}^3}\mu u + 0.292\frac{(S_v)}{\varepsilon_{tot}^3}\rho_{gas}u^2 \tag{12}$$

For packed beds of spherical particles the specific surface area can be expressed as $S_v = 6(1\text{-}\varepsilon)/d_{pellet}$: by performing this substitution the more common form of the equation can be derived. As shown in Fig. 7, such a correlation matches well the experimental data collected for the packed bed in the present work.

As proposed for packed foams [35], we herein assume a close analogy of packed POCS with packed beds in order to derive an Ergun-type equation for pressure drop in packed POCS. Accordingly, the total porosity (ε_{tot} from Eq. (11)) and the total surface area of both pellets and structured internals $S_{v,tot}$ were considered in Eq. (12). The surface area correlations for POCS ($S_{v,POCS}$) with cubic and diamond/Kelvin unit cells were taken from literature [37,38]. For the pellets, the surface area ($S_{v,Packing}$) was calculated from Eq. (13), considering the porosity inside the structure and the ratio between volume available for the packing and the total volume. The total wetted surface area is the sum of the areas of the structure and of the particles (Eq. (14)).

$$S_{v,packing} = \frac{6(1 - \varepsilon_{Packing})}{d_{pellet}}\varepsilon_{POCS} \tag{13}$$

$$S_{v,tot} = S_{v,POCS} + S_{v,Packing} \tag{14}$$

Fig. 7 shows an excellent agreement between the collected experimental data and the proposed correlation, which is able to match the data with great accuracy for all investigated structures. A comprehensive comparison of the experimental data and the proposed correlation is shown as a parity plot in Fig. 8.

For all investigated POCS with different unit cells, the correlation based on Eqs. (12)–(14) seems to provide a reasonable estimate of the pressure drop, with mean average percentage errors (MAPE) lower than 10 % and maximum errors below ± 30 %.

3.3. Heat transfer in packed POCS

3.3.1. Experimental temperature profiles

Temperature profiles were collected during heat transfer (heating) runs in packed bed and packed POCS configurations to provide an experimental basis for the assessment of the heat transfer performances.

A qualitative description of the experimental findings associated with the adoption of packed POCS is possible by comparing the temperature profiles collected at Q = 35 NLM, $T_{oil,set}$ = 150 °C for the

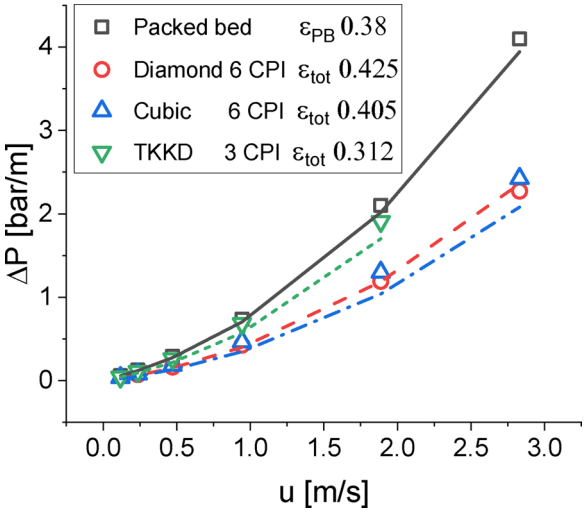

Fig. 7. Comparison of pressure drop in a packed bed and in three POCS packed with the same pellets of d_{pellet} = 600 μm. Symbols represent the experimental data, lines the proposed correlation for the packed bed and packed POCS, respectively (Eqs. (12)–(14)).

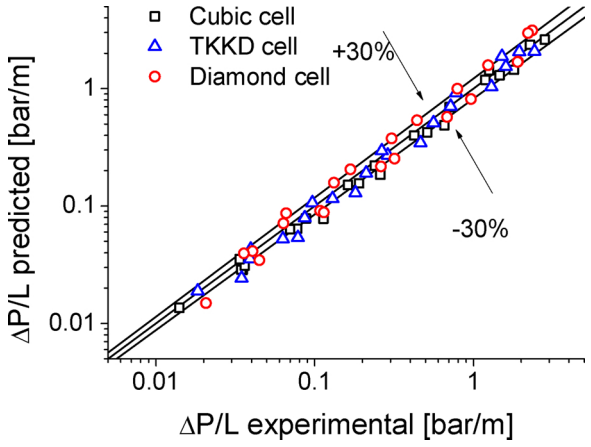

Fig. 8. Parity plot: Collected experimental data versus the proposed correlation, Eq. (12).

different systems displayed in Fig. 9. These tests were performed with the same pellets (1 mm glass beads) and with three different metallic POCS, a 5 CPI cubic cell Ti-alloy POCS with $\varepsilon_{POCS} = 0.94$, a 5 CPI cubic cell aluminum POCS with $\varepsilon_{POCS} = 0.92$ and a cubic cell Ti-alloy POCS characterized by 7 CPI and $\varepsilon_{POCS} = 0.86$.

The temperature profile of the packed bed (a) shows the expected features: strong radial gradients are present both inside the bed among the three internal profiles, associated with the poor radial effective thermal conductivity, and between the wall and the lateral profile, associated with a significant heat transfer resistance at the wall.

In the case of the poorly conductive packed POCS (5 CPI Titanium alloy (b)), only a small improvement in the temperature profile is evident. The radial temperature differences between the three internal thermocouples were similar to the previous case, and also the difference between the wall and the lateral temperature was only slightly reduced.

Temperature profiles obtained with the conductive POCS (5 CPI, Aluminum alloy (c)) are quite different from the others. Much flatter radial temperature profiles are present in the core of the bed thanks to the improved effective thermal conductivity, whereas at the wall the temperature difference was similar to cases (a) and (b).

The last panel of Fig. 9 (d) shows the temperature profile of a poorly conductive (Ti-alloy) POCS characterized by a smaller cell size (7 CPI) and lower porosity than the structures used in cases (b)-(c). In this test, the radial temperature differences in the core of the bed are quite high due to the comparatively poor thermal conductivity of the used metal. In the peripheral region, however, a reduction of the temperature gap between the wall and the temperature at r = 10 mm is evident. The same qualitative considerations apply also to data collected at different flow rates.

By data comparison it is possible to envision some effects on the overall heat transfer performance of the system. A high thermal conductivity of the POCS material helps in increasing the radial and axial effective thermal conductivity. In addition, an effect of the geometry of the support is also present, particularly in the wall region, and should therefore be considered in the development of a generalized heat transfer model for these systems.

3.3.2. *Evaluation of the heat transfer coefficients*

In order to quantify the overall heat transfer performance of the packed POCS, a 1D model analysis was performed.

Eq. (15) provides the steady-state 1D energy balance in temperature

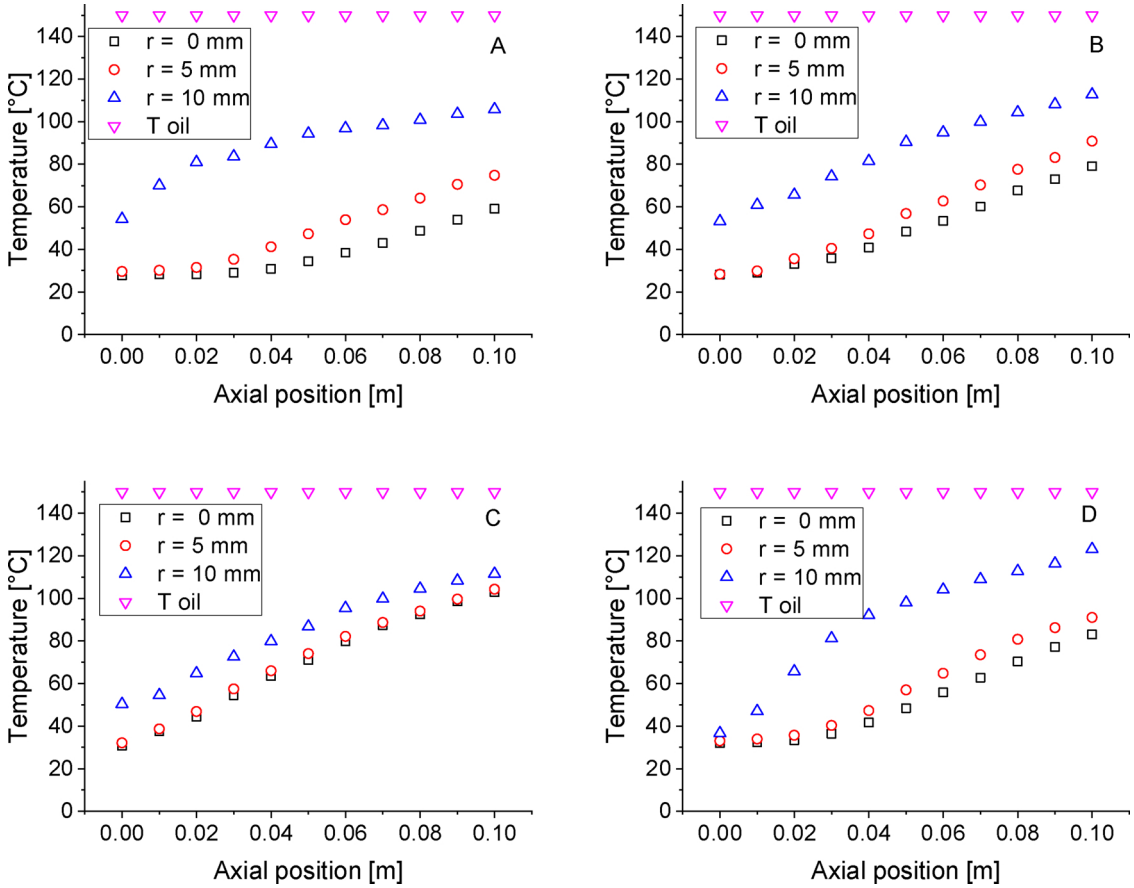

Fig. 9. Temperature profiles collected at 35 NLM using glass beads as packing: a) packed bed, b) packed POCS cubic cell 5 CPI Ti-alloy $\varepsilon = 0.94$, c) cubic cell 5 CPI Al-alloy $\varepsilon = 0.92$, d) cubic cell 7 CPI Ti-alloy $\varepsilon = 0.86$.

form for a fluid flowing through a heated/cooled pipe:

$$\rho_{gas} u c_p \frac{dT_c}{dz} = \frac{4}{d_t} U (T_{oil} - T_c) \quad (15)$$

where T_c is the mean-cup temperature of the fluid. The cupmix temperature for each axial point can be calculated as in Eq. (16) under the assumptions of negligible dependency of the gas heat capacity on temperature and of ideal plug flow behavior:

$$T_c = \frac{2\int_o^{r_t} T(r) r\, dr}{r_t^2} \quad (16)$$

For the evaluation of T_c it is then necessary to describe the radial temperature profile for each axial coordinate z. For each point (11 points in axial direction, 1 cm spacing), the temperatures at r = 0, r = 5 mm and r = 10 mm are measured. The radial temperature profiles were then evaluated by interpolating the data with the 4th order symmetric polynomial in Eq. (17):

$$T(r) = T(r=0) + ar^2 + br^4 \quad (17)$$

Assuming constant fluid properties, the analytical solution of Eq. (15) is given by:

$$T_c(z) = T_{oil} - (T_{oil} - T_{c,z=0}) \exp^{\frac{-4Uz}{\rho u c_p d_t}} \quad (18)$$

By linearization of the proposed equation, it is possible to estimate the overall heat transfer coefficient U by linear regression analysis of the experimental temperature data.

The heat transfer coefficient U in Eq. (18) also includes the contribution of the external heat transfer coefficient, which refers to the oil heated jacket and is not of general interest, being specific for the test rig adopted in the present study. An external coefficient $h_{w,oil,wall}$ = 350 W/m^2/K was calculated from the specifications of the heating systems using the correlations reported in the VDI Wärmeatlas [42]. With this value, it is possible to evaluate the 1D heat transfer coefficient associated with the effective radial conductivity and the internal wall heat transfer resistance as reported in Eq. (19).

$$U_{overall} = \left(\frac{1}{U} - \frac{1}{h_{w\,oil,wall}} \right)^{-1} \quad (19)$$

The presence of such an additional resistance between the heating oil and the catalyst bed has a very modest impact on tests with packed beds at low flow rates. However, it has a significant and non-negligible effect on the experimental tests performed with packed POCS at high flow rates, and therefore it needs to be carefully considered in the evaluation of the heat transport properties of POCS.

3.3.3. Comparison of the overall heat transfer coefficients

The estimates of the overall heat transfer coefficient are plotted in Fig. 10 as a function of the flow rate. For all the investigated systems, the overall heat transfer coefficient increases with increasing flow rate Q. Packed POCS show a clear enhancement of the overall heat transfer coefficient with respect to the packed bed in the whole investigated range of flow rates. From this chart it is evident that both, the geometry of the structure and the thermal conductivity of the POCS material play a relevant role for the heat transfer performance. An engineering model able to reflect all these features is therefore essential for a realistic evaluation of the proposed solution of conductive packed POCS.

3.3.4. Development and validation of a heat transport model for packed POCS

Following the approach already adopted for packed foams [3,34], heat transfer in packed POCS can be represented by the equivalent thermal circuit displayed in Fig. 11. The circuit is derived under the assumption that packed POCS can be represented by two distinct phases, namely the POCS solid network and a single pseudo-homogeneous phase, i.e., lumping the fluid phase and the particles, in analogy to the established pseudo-homogeneous modelling approaches in literature on packed beds. To assess the heat transfer in non-reactive heating and cooling experiments under the assumption that the measured temperature is the one of the lumped phase, the following scheme is considered.

Following the heat flux from the wall to the core of the gas/particle phase, the first part of the circuit consists of two resistances connected in parallel at the wall, one associated with the effective gap between the POCS and the wall, the other associated with the wall heat transfer of the packed particles. For the description of the heat flux from the near wall region to the core of the bed either a mainly convective mechanism through the gas/packed particle pseudo-homogeneous phase or conduction through the connected solid framework of the POCS is assumed. In the latter path, an additional resistance for the heat transfer between the solid POCS and the pseudo-homogeneous phase needs to be considered in series to the resistance of the structure.

We have estimated all the individual terms of the equivalent circuit shown in Fig. 11 according to literature correlations. For the POCS heat transfer coefficient, the static term of the correlation proposed by Busse et al. [4] has been considered:

$$h_{w,POCS} = \frac{Nu_{static}\, k_{gas}}{d_{cell}} \quad (20)$$

In this Eq. (20), Nu_{static} = 4.51 was assumed for cubic cells [4], while other values should be adopted for POCS with different unit cell shapes.

For the packed bed, the wall heat transfer coefficient has been evaluated according to Specchia et al. [43] for both the static and the convective term:

$$h_{w,Packing}\ static = \left(\frac{k_{gas}}{d_{pellet}}\right)\left(2\varepsilon_{Packing} + \frac{1-\varepsilon_{Packing}}{0.0024}\left(\frac{d_t}{d_{pellet}}\right)^{1.58} + \frac{1}{3}\frac{k_{gas}}{k_{pellet}}\right) \quad (21)$$

$$\mathrm{Re}_{particle}<1200 \quad h_{w,Packing}\ convective = \left(\frac{k_{gas}}{d_{pellet}}\right) 0.0835\, \mathrm{Re}^{0.91} \quad (22)$$

$$\mathrm{Re}_{particle}>1200 \quad h_{w,Packing}\ convective = \left(\frac{k_{gas}}{d_{pellet}}\right) 1.23\, \mathrm{Re}^{0.51} \quad (23)$$

The parallel connection of the POCS and the packed bed contributions results in the following overall wall heat transfer resistance:

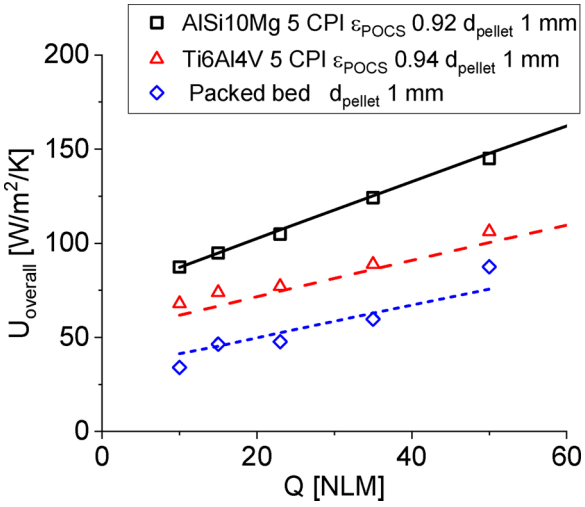

Fig. 10. Experimental overall heat transfer coefficients against model estimates (Eqs. (20)–(33)).

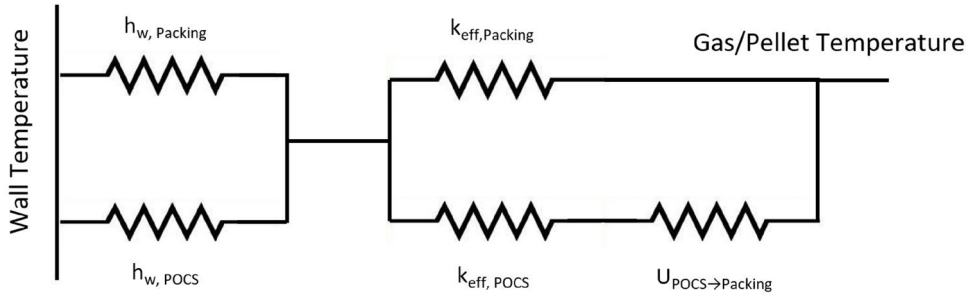

Fig. 11. Schematic representation of the heat transfer pathways in packed POCS.

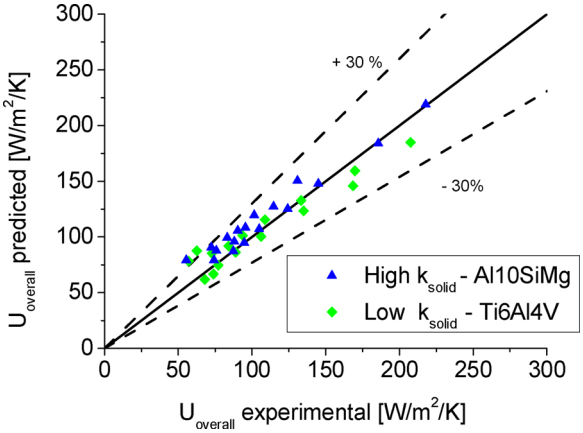

Fig. 12. Parity plot: collected packed POCS data against the proposed heat transfer model.

$$R_{wall} = \left(\frac{1}{h_{w,POCS} + h_{w,Packing}\, static + h_{w,Packing}\, convective} \right) \tag{24}$$

Concerning the internal resistances, the effective thermal conductivity of the POCS is not influenced by the presence of the packing since it is dominated by heat conduction in the solid matrix. Bianchi et al. [25] performed a numerical study of the effective thermal conductivity of POCS and derived Eq. (25), which has been adopted in this work:

$$k_{eff,POCS} = k_{solid,\,POCS}\,[0.36 + 0.64(1 - \varepsilon_{POCS})](1 - \varepsilon_{POCS}) \tag{25}$$

The effective radial thermal conductivity of the packed bed was calculated using the correlations proposed by Specchia et al. [43], which include both static and convective terms:

$$k_{eff,Packing}\,\text{static} = (1\text{-}\varepsilon_{\text{POCS}}) \left[k_{gas}\varepsilon_{Packing} + \frac{k_{gas}(1 - \varepsilon_{Packing})}{0.22\varepsilon_{Packing}^2 + \frac{2}{3}\frac{k_{gas}}{k_{pellet}}} \right] \tag{26}$$

$$k_{eff,Packing}\,convective = k_{gas}\frac{RePr}{Pe_{rif}} \tag{27}$$

$$Pe_{rif} = 8.65\left[1 + 19.4\left(\frac{d_{pellet}}{d_t}\right)^2\right] \tag{28}$$

Finally, the interphase heat transfer resistance was computed by introducing the internal heat transfer coefficient $U_{\text{POCS-Packing}}$. The heat transfer between the two phases is regulated by the heat transfer coefficients and the surface area of the POCS.

$$R_{IF} = \frac{4}{d_t S_{v,POCS} U_{POCS \to Packing}} \tag{29}$$

The calculation of $U_{\text{POCS- > Packing}}$ is based on the same correlations proposed by Specchia et al. [43] applied to a virtual channel with a diameter equal to d_{cell}.

The total internal resistance is evaluated by connecting in parallel the internal resistances of the packed bed, R_p

$$R_P = \frac{d_t}{6.13(k_{eff,Packing\text{static}} + k_{eff,Packing\text{convective}})} \tag{30}$$

with the series of the resistances associated with the POCS matrix (Eq. (25)),

$$R_{POCS} = \frac{d_t}{6.13(k_{eff,POCS})} \tag{31}$$

and with the internal resistance, $R_{IF,}$ as reported in Eq. (29).

$$R_{INT} = \frac{R_P(R_{POCS} + R_{IF})}{R_P + (R_{POCS} + R_{IF})} \tag{32}$$

Finally, the overall heat transfer coefficient of the whole system is computed as given in Eq. (33).

$$U_{overall} = (R_{WALL} + R_{INT})^{-1} \tag{33}$$

Estimates provided by this predictive model are compared with overall heat transfer coefficients determined from experiments for different pairs of pellets and structures as shown in Fig. 10. The proposed heat transfer model can predict the measured experimental data without any fitting coefficient and is clearly able to reflect all the experimentally observed behavior for the different systems.

As a summary, Fig. 12 displays a parity plot with the systematic comparison of the proposed heat transfer model and the collected experimental data, including the whole set of investigated conditions and pellet-structures combinations. Data are grouped in terms of highly conductive structures and poorly conductive structures to assess the adequacy of the model to estimate the overall heat transfer coefficients in both cases. The agreement between the proposed model and the experimental data is remarkable, especially in the case of highly conductive structures. The proposed model can therefore be used as a predictive tool for estimating the heat transfer properties of packed POCS.

To gain insight into the impact of the POCS internals' contribution to the overall heat transfer coefficient, calculations were performed with the proposed model for 5 CPI cubic cell POCS filled with 1 mm particles. Structures made either of Ti6Al4V alloy or of AlSi10Mg alloy were considered as representative examples of poorly conductive and highly conductive materials tested in the experimental campaign,

Table 4
Properties used for the calculations of Fig. 13.

Tube diameter	25.4 mm	Gas	Air
Pellet diameter	1 mm	Temperature	200 °C
POCS cell size	5 mm	Pressure	1 bar
POCS porosity	0.9	Cp	1.05 kJ/kg/K
Pellet thermal conductivity	0.3 W/m/K	Gas thermal conductivity	0.0377 W/m/K

respectively. Pellets with a thermal conductivity of 0.3 W/m/K and a tube with a diameter equal to 2.54 cm (similar to the experimental setup) were assumed. Other relevant properties used for the simulations are listed in Table 4.

The calculated trends of $U_{overall}$ are plotted versus the specific mass flow rate G in Fig. 13a). It can be observed that the packed bed and the Ti-alloy packed POCS display parallel trends of $U_{overall}$ on increasing the specific mass flow rate. In this comparison, the Ti-alloy packed POCS offer a moderate increase of the static contribution (both at the wall and for the effective conductivity term) resulting in a slightly higher overall heat transfer coefficient. Accordingly, the impact of the static contribution on the total heat transfer coefficient as shown in Fig. 13b) is higher than for the packed bed reactor case. When POCS made of AlSi10Mg alloy as representative of highly conductive internals are considered, the overall heat transfer rate is higher over the whole investigated range of specific mass flow rates. This is due to the high effective thermal conductivity of the POCS which almost suppresses the internal heat transfer resistance. However, when, computing the impact of the static contribution on the overall heat transfer (Fig. 13b), we found that it is higher than for packed bed reactors, but lower than for the Ti-alloy case. This is consistent with the steeper slope of $U_{overall}$ observed in Fig. 13 a. When using a highly conductive internal, in fact, the controlling resistances are shifted to the wall and to the gas (actually the fluid/packed spheres pseudo-phase)/solid heat transfer terms, that, as described above, both include a static and a convective contribution, which are responsible for the observed trends.

3.4. Packed POCS versus packed beds as enhanced catalytic reactor configuration

In order to assess the potential of coated POCS as catalyst carriers Busse et al. [4] compared the overall heat transfer coefficients of bare POCS with those of packed beds at varying specific mass flow rates G and thermal conductivity of the POCS material. Results show that conductive bare POCS provide a significant advantage in air at low mass flow rates, while they exhibit lower overall heat transfer coefficients than packed beds for higher mass flow rates of $G > 2.5$ kg/m^2/s.

In the present contribution, the analysis is extended to the packed POCS configuration. For one, the same gas properties (air) and tube diameter (2.54 cm) as used by Busse et al. [4] were adopted in the calculations. As a second case, syngas was also considered. A cubic cell POCS with $d_{cell} = 8$ mm and $\varepsilon = 0.9$ packed with particles of 2 mm diameter ($\varepsilon_{packing} = 0.44$) was investigated. Details of the properties assumed are reported in Table 5.

Fig. 14 shows the ratio of the overall heat transfer coefficient of the packed POCS and the packed beds illustrated by the color code and plotted against the specific mass flow rate and the intrinsic thermal conductivity of the POCS material.

From Fig. 14 it is possible to assess that packed POCS made of conductive material provide a significant advantage for the intensification of heat transfer rates at low mass flow rates, as highlighted also by Fig. 13. Besides, thanks to the synergy of the respective heat transfer mechanisms dominant in POCS (i.e. conduction) and in packed beds (i.e. convective heat transfer), the proposed solution is competitive also at higher flow rates, showing an advantage of at least 20 % in case of aluminum POCS at industrial flow rates. For the same reactor geometries and packing, the advantages are even more pronounced in case of a conductive gas, since it is possible to reduce the heat transfer limitations at the wall which are characteristic of structured catalysts.

Finally, on the basis of the collected results, a realistic process scenario was analyzed to better assess the potential of these structures. The data of a Sabatier pilot reactor [44] as reported in Table 6 were considered. From the given mass flow rate, the catalyst mass and the tube diameter a tube length of 3 m was derived assuming a packed bed porosity of 0.4.

For the packed POCS (AlSi10Mg, cubic cells) configuration, a constrained multivariable optimization was performed to maximize the overall heat transfer coefficient, fixing the tube length at 3.5 and 3.75 m respectively, and constraining the tube catalyst inventory and the overall pressure drop to be equal to those of the packed bed reactor.

The results in Fig. 15 show that progressive increments of the overall heat transfer coefficient up to over 30 % are obtained with the packed POCS when allowing for an increment of the tube length of 15–25 %. The lower packing density in POCS results in a lower pressure drop per unit length, which allows to comply with the constraint on the total pressure drop.

The aim of this section is to briefly demonstrate how packed POCS can be designed and adapted to strongly enhance the heat transfer rates over a broad range of mass flow rates and process conditions by keeping the same catalyst mass and pressure drop of the reactor. The increased heat transfer could be in principle coupled with the adoption of a more active catalyst to improve the process performance and/or may enable the use of larger tubes, thereby reducing the number of tubes. Of course, a rigorous reactor optimization based on the proposed solution of packed POCS should consider a more detailed model accounting for reaction kinetics, internal mass transport processes and external wall temperature conditions.

4. Conclusions

In this work, packed periodic open cellular structures (POCS) made of thermally conductive materials are introduced and proposed as a

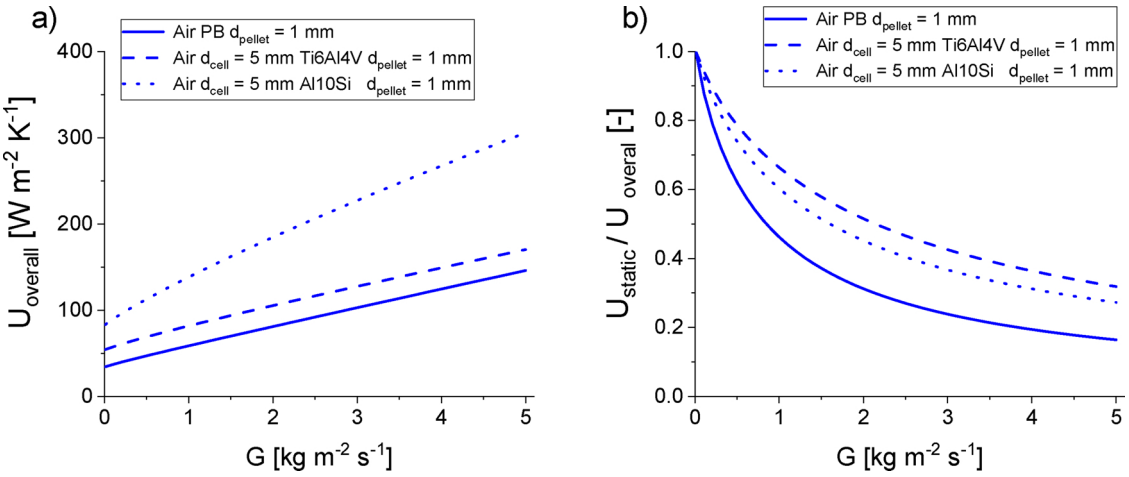

Fig. 13. Comparison of overall heat transfer coefficients of packed POCS in air for 5 CPI POCS.

Table 5
Properties used for the calculations of Fig. 14.

Tube diameter	25.4 mm	Gas	Air	Syngas H_2/CO = 2
Pellet diameter	1 mm	Temperature	200 °C	200 °C
POCS cell size	5 mm	Pressure	1 bar	25 bar
POCS porosity	0.9	c_p	1.05 kJ/kg/K	2.5 kJ/kg/K
Pellet thermal conductivity	1 W/m/K	Gas thermal conductivity	0.0377 W/m/K	0.133 W/m/K

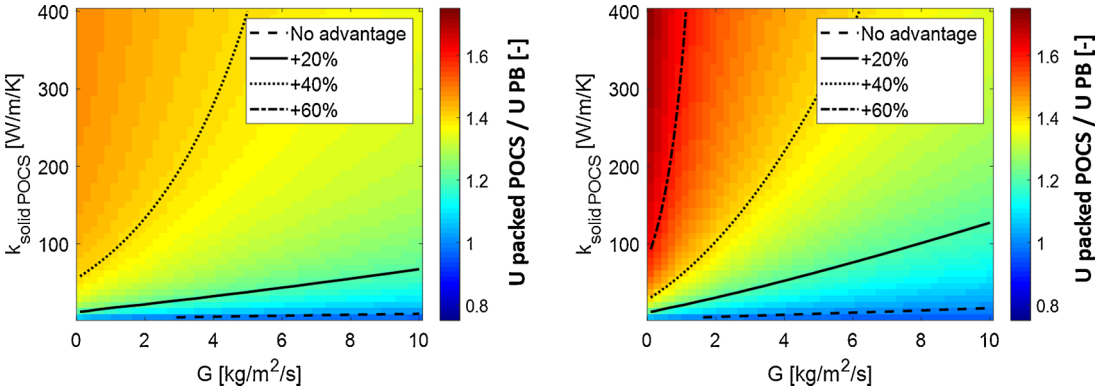

Fig. 14. Comparison of overall heat transfer coefficients of packed POCS and packed beds in function of the specific mass flow rate G and the solid thermal conductivity k_s. Left: air, right: syngas.

Table 6
Properties used for the CO_2 methanation case study.

Tube diameter	30 mm	Gas composition (inlet)	H_2/CO_2 = 4
Pellet diameter	3 mm	Pressure	10 bar
Pellet thermal conductivity	1 W/m/K	G – Specific mass flow rate	1.98 kg/m^2/s
POCS thermal conductivity	150 W/m/K	Gas thermal conductivity	0.183 W/m/K

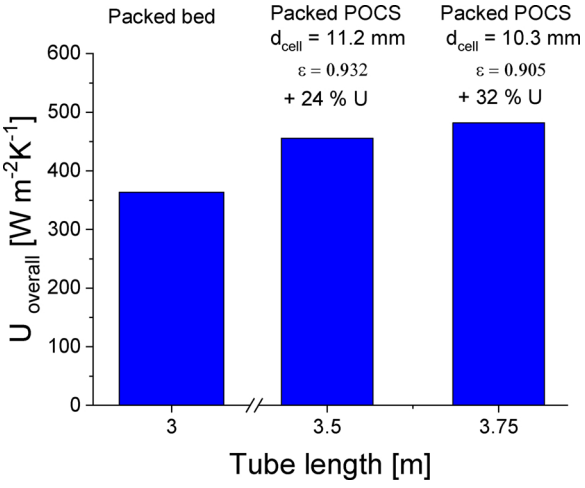

Fig. 15. Comparison of overall heat transfer coefficients of optimized reactors for CO_2 methanation.

promising solution for the intensification of catalytic processes. Thanks to the design freedom offered by additive manufacturing of the POCS, this solution enables to enhance heat transfer rates in tubular reactors while using conventional industrial-scale catalyst pellets. This feature is important for practical applications, and therefore represents an important advantage of packed POCS over the recently proposed concept of packed foams where typically smaller pellets have to be used.

The main design parameters of the proposed solution of packed POCS were analyzed in detail in this study. First, the packing efficiency as a function of the ratio of the structure window size to the pellet size was investigated, and a descriptive correlation that can be adopted for the design of structures able to host the given amount of catalyst per unit reactor volume was developed. Then, the pressure drop in the proposed systems was studied experimentally. Depending on the total porosity of the system, packed POCS may show similar or lower pressure drop compared to conventional packed bed reactors. The well-known Ergun correlation was adapted in order to describe predictively the pressure drop in the systems. The last part of the work was devoted to study the heat transfer performance of the packed POCS in presence of both poorly conductive and highly conductive structures. The experimental study revealed the strong impact of both the thermal conductivity of the POCS and the geometry of the internals on the overall heat transfer rates. A comprehensive predictive heat transfer model that reflects the principle physics of the system was developed by appropriate combination and adaptation of selected literature correlations for the individual parameters. The model is able to reflect all the effects observed in the experiments and can predict the heat transfer performance of the system with a high level of accuracy.

Based on the developed correlations, a case study has highlighted the potential of packed POCS by comparing the overall heat transfer rates with those of a conventional packed bed at fixed catalyst inventory and pressure drop. The identified potential for substantially increasing the heat transfer rates associated with the adoption of these solutions over a broad range of operating conditions clearly illustrates that the proposed concept of packed POCS is an interesting option for process intensification.

CRediT authorship contribution statement

Matteo Ambrosetti: Data curation, Methodology, Investigation, Software, Validation, Formal analysis, Visualization, Writing - original

draft. **Gianpiero Groppi:** Conceptualization, Methodology, Resources, Writing - review & editing, Supervision. **Wilhelm Schwieger:** Conceptualization, Resources, Funding acquisition. **Enrico Tronconi:** Conceptualization, Resources, Writing - review & editing, Supervision, Project administration, Funding acquisition. **Hannsjörg Freund:** Conceptualization, Resources, Writing - review & editing, Supervision, Project administration, Funding acquisition.

Declaration of Competing Interest

The authors declare that they have no known competing financial interests or personal relationships that could have appeared to influence the work reported in this paper.

Acknowledgement

The authors from Politecnico di Milano acknowledge the European Research Council for Grant Agreement 694910 (INTENT). The authors from FAU acknowledge financial support from the Bavarian Ministry of Economic Affairs and Media, Energy and Technology within the framework of the Technology Transfer Center VerTec in Fürth as well as funding of the German Research Foundation (DFG) for the Cluster of Excellence "Engineering of Advanced Materials" at FAU Erlangen-Nürnberg. The authors from Politecnico di Milano want to thank Sasol for providing the pellet samples.

References

[1] A.G. Dixon, Correlations for wall and particle shape effects on fixed bed bulk voidage, Can. J. Chem. Eng. 66 (1988) 705–708, https://doi.org/10.1002/cjce.5450660501.
[2] V. Specchia, S. Sicardi, Modified correlation for the conductive contribution of thermal conductivity in packed bed reactors, Chem. Eng. Commun. 6 (1980) 131–139, https://doi.org/10.1080/00986448008912525.
[3] C.G. Visconti, G. Groppi, E. Tronconi, Highly conductive "packed foams": a new concept for the intensification of strongly endo- and exo-thermic catalytic processes in compact tubular reactors, Catal. Today 273 (2015) 178–186, https://doi.org/10.1016/j.cattod.2016.02.060.
[4] C. Busse, H. Freund, W. Schwieger, Intensification of heat transfer in catalytic reactors by additively manufactured periodic open cellular structures (POCS), Chem. Eng. Process. - Process Intensif. 124 (2018) 199–214, https://doi.org/10.1016/j.cep.2018.01.023.
[5] R. Berger, EUROKIN Spreadsheet on Requirements for Measurement of Intrinsic Kinetics in the Gas-solid Fixed Bed Reactors, (2020) available at http://eurokin.org/?page_id=571.
[6] A. Cybulski, J.A. Moulijn, Structured Catalysts and Reactors, 2nd ed., CRC Press, 2005, p. 856, https://doi.org/10.1201/9781420028003.
[7] S. Danaci, L. Protasova, J. Lefevere, L. Bedel, R. Guilet, P. Marty, Efficient CO_2 methanation over Ni/Al2O3coated structured catalysts, Catal. Today 273 (2016) 234–243, https://doi.org/10.1016/j.cattod.2016.04.019.
[8] T. Stiegler, K. Meltzer, A. Tremel, M. Baldauf, P. Wasserscheid, J. Albert, Development of a structured reactor system for CO2 methanation under dynamic operating conditions, Energy Technol. 7 (2019) 1–12, https://doi.org/10.1002/ente.201900047.
[9] T.J. Schildhauer, E. Newson, A. Wokaun, Closed cross flow structures-improving the heat transfer in fixed bed reactors by enforcing radial convection, Chem. Eng. Process. - Process Intensif. 48 (2009) 321–328, https://doi.org/10.1016/j.cep.2008.04.009.
[10] E. Hansjosten, A. Wenka, A. Hensel, W. Benzinger, M. Klumpp, R. Dittmeyer, Custom-designed 3D-printed metallic fluid guiding elements for enhanced heat transfer at low pressure drop, Chem. Eng. Process. - Process Intensif. 130 (2018) 119–126, https://doi.org/10.1016/j.cep.2018.05.022.
[11] J. De Wilde, G.F. Froment, Computational fluid dynamics in chemical reactor analysis and design: application to the zoneflow^{TM} reactor for methane steam reforming, Fuel 100 (2012) 48–56, https://doi.org/10.1016/j.fuel.2011.08.068.
[12] E. Tronconi, G. Groppi, T. Boger, A. Heibel, Monolithic catalysts with "high conductivity" honeycomb supports for gas/solid exothermic reactions: characterization of the heat-transfer properties, Chem. Eng. Sci. 59 (2004) 4941–4949, https://doi.org/10.1016/j.ces.2004.07.018.
[13] G. Groppi, E. Tronconi, C. Cortelli, R. Leanza, Conductive monolithic catalysts: development and industrial pilot tests for the oxidation of o-xylene to phthalic anhydride, Ind. Eng. Chem. Res. 51 (2012) 7590–7596, https://doi.org/10.1021/ie2021653.
[14] G. Kolb, Review: Microstructured reactors for distributed and renewable production of fuels and electrical energy, Chem. Eng. Process. - Process Intensif. 65 (2013) 1–44, https://doi.org/10.1016/J.CEP.2012.10.015.
[15] A. Holmen, H.J. Venvik, R. Myrstad, J. Zhu, D. Chen, Monolithic, microchannel and carbon nanofibers/carbon felt reactors for syngas conversion by Fischer-Tropsch synthesis, Catal. Today 216 (2013) 150–157, https://doi.org/10.1016/j.cattod.2013.06.006.
[16] G. Liesche, K. Sundmacher, Productivity versus product quality: exploring the limits of autothermal microchannel reactors in methane steam reforming, Chem. Eng. J. (2018) 0–1, https://doi.org/10.1016/j.cej.2018.09.209.
[17] S. Bac, S. Keskin, A.K. Avci, Modeling and simulation of water-gas shift in a heat exchange integrated microchannel converter, Int. J. Hydrogen Energy 43 (2018) 1094–1104, https://doi.org/10.1016/j.ijhydene.2017.09.141.
[18] E. Bianchi, T. Heidig, C.G. Visconti, G. Groppi, H. Freund, E. Tronconi, An appraisal of the heat transfer properties of metallic open-cell foams for strongly exo-/endothermic catalytic processes in tubular reactors, Chem. Eng. J. 198–199 (2012) 512–528, https://doi.org/10.1016/j.cej.2012.05.045.
[19] A. Montebelli, C.G. Visconti, G. Groppi, E. Tronconi, C. Ferreira, S. Kohler, Enabling small-scale methanol synthesis reactors through the adoption of highly conductive structured catalysts, Catal. Today 215 (2013) 176–185, https://doi.org/10.1016/j.cattod.2013.02.020.
[20] P.S. Roy, J. Song, K. Kim, J.M. Kim, C.S. Park, A.S.K. Raju, Effects of CeZrO2–Al2O3 support composition of metal-foam-coated Pd–Rh catalysts for the steam-biogas reforming reaction, J. Ind. Eng. Chem. 62 (2018) 120–129, https://doi.org/10.1016/j.jiec.2017.12.050.
[21] D. Merino, O. Sanz, M. Montes, Effect of the thermal conductivity and catalyst layer thickness on the Fischer-Tropsch synthesis selectivity using structured catalysts, Chem. Eng. J. 327 (2017) 1033–1042, https://doi.org/10.1016/J.CEJ.2017.07.003.
[22] E. Verlato, S. Barison, S. Cimino, F. Dergal, L. Lisi, G. Mancino, M. Musiani, L. Vàzquez-Gòmez, Catalytic partial oxidation of methane over nanosized Rh supported on Fecralloy foams, Int. J. Hydrogen Energy 39 (2014) 11473–11485, https://doi.org/10.1016/j.ijhydene.2014.05.076.
[23] L. Kiewidt, J. Thöming, Pareto-optimal design and assessment of monolithic sponges as catalyst carriers for exothermic reactions, Chem. Eng. J. 359 (2019) 496–504, https://doi.org/10.1016/j.cej.2018.11.109.
[24] A. Inayat, J. Schwerdtfeger, H. Freund, C. Körner, R.F. Singer, W. Schwieger, Periodic open-cell foams: pressure drop measurements and modeling of an ideal tetrakaidecahedra packing, Chem. Eng. Sci. 66 (2011) 2758–2763, https://doi.org/10.1016/j.ces.2011.03.031.
[25] E. Bianchi, W. Schwieger, H. Freund, Assessment of periodic open cellular structures for enhanced heat conduction in catalytic fixed-bed reactors, Adv. Eng. Mater. 18 (2016) 608–614, https://doi.org/10.1002/adem.201500356.
[26] M. Bracconi, M. Ambrosetti, M. Maestri, G. Groppi, E. Tronconi, A fundamental analysis of the influence of the geometrical properties on the effective thermal conductivity of open-cell foams, Chem. Eng. Process. - Process Intensif. 129 (2018) 181–189, https://doi.org/10.1016/j.cep.2018.04.018.
[27] N.F. Bastos Rebelo, K.A. Andreassen, L.I. Suarez Ríos, J.C. Piquero Camblor, H.J. Zander, C.A. Grande, Pressure drop and heat transfer properties of cubic isoreticular foams, Chem. Eng. Process. - Process Intensif. 127 (2018) 36–42, https://doi.org/10.1016/j.cep.2018.03.008.
[28] B.W. Van Hasselt, D.J. Lindenbergh, H.P. Calis, S.T. Sie, C.M. Van Den Bleek, The three-levels-of-porosity reactor. A novel reactor for countercurrent trickle-flow processes, Chem. Eng. Sci. 52 (1997) 3901–3907, https://doi.org/10.1016/S0009-2509(97)00234-0.
[29] K. Pangarkar, T.J. Schildhauer, J.R. van Ommen, J. Nijenhuis, J.A. Moulijn, F. Kapteijn, Experimental and numerical comparison of structured packings with a randomly packed bed reactor for Fischer-Tropsch synthesis, Catal. Today 147 (2009) 2–9, https://doi.org/10.1016/j.cattod.2009.07.035.
[30] T.J. Schildhauer, K. Pangarkar, J.R. van Ommen, J. Nijenhuis, J.A. Moulijn, F. Kapteijn, Heat transport in structured packings with two-phase co-current downflow, Chem. Eng. J. 185–186 (2012) 250–266, https://doi.org/10.1016/j.cej.2011.11.054.
[31] G. Groppi, E. Tronconi, C.G. Visconti, A. Tasso, R. Zennaro, Packed-Bed Tubular Reactor For Heterogeneous Exothermic Or Endothermic Catalytic Reactions, US20160208175 (2015).
[32] L. Fratalocchi, C.G. Visconti, G. Groppi, L. Lietti, E. Tronconi, Intensifying heat transfer in Fischer-Tropsch tubular reactors through the adoption of conductive packed foams, Chem. Eng. J. 349 (2018) 829–837.
[33] R. Balzarotti, A. Beretta, G. Groppi, E. Tronconi, A comparison between washcoated and packed copper foams for the intensification of methane steam reforming, React. Chem. Eng. 4 (2019) 1387–1392, https://doi.org/10.1039/c9re00125e.
[34] R. Balzarotti, M. Ambrosetti, A. Beretta, G. Groppi, E. Tronconi, Investigation of packed conductive foams as a novel reactor configuration for methane steam reforming, Chem. Eng. J. (2019) 123494, https://doi.org/10.1016/j.cej.2019.123494.
[35] M. Ambrosetti, M. Bracconi, M. Maestri, G. Groppi, E. Tronconi, Packed foams for the intensification of catalytic processes: assessment of packing efficiency and pressure drop using a combined experimental and numerical approach, Chem. Eng. J. 382 (2020) 122801, https://doi.org/10.1016/j.cej.2019.122801.
[36] G. Belussi, M. Bohnet, J. Bus, K. Drautz, H. Greim, K.-P. Jackel, U. Karts, A. Kleeman, G. Kreysa, T. Laird, W. Meier, E. Ottow, M. Roper, J. Scholtz, K. Sundmaker, R. Ulber, U. Wietelmann, 7th ed., Ullmann's Encyclopedia of Industrial Chemistry 40 Vol. Set (2011).
[37] M. Klumpp, A. Inayat, J. Schwerdtfeger, C. Körner, R.F. Singer, H. Freund, W. Schwieger, Periodic open cellular structures with ideal cubic cell geometry: effect of porosity and cell orientation on pressure drop behavior, Chem. Eng. J. 242 (2014) 364–378, https://doi.org/10.1016/j.cej.2013.12.060.
[38] M. Lämmermann, G. Horak, W. Schwieger, H. Freund, Periodic open cellular structures (POCS) for intensification of multiphase reactors: liquid holdup and two-

phase pressure drop, Chem. Eng. Process. - Process Intensif. 126 (2018) 178–189, https://doi.org/10.1016/j.cep.2018.02.027.
[39] C. Parra-Cabrera, C. Achille, S. Kuhn, R. Ameloot, 3D printing in chemical engineering and catalytic technology: structured catalysts, mixers and reactors, Chem. Soc. Rev. 47 (2018) 209–230, https://doi.org/10.1039/c7cs00631d.
[40] S. Ergun, Fluid flow through packed columns, Chem. Eng. Prog. 48 (1952) 89–94 doi:citeulike-article-id:7797897.
[41] S. Ergun, A.A. Orning, Fluid flow through randomly packed columns and fluidized beds, Ind. Eng. Chem. 41 (1949) 1179–1184, https://doi.org/10.1021/ie50474a011.
[42] VDI-Gesellschaft Verfahrenstechnik und Chemieingenieurwesen, ed., VDI Heat Atlas, Second edition, 2010.
[43] V. Specchia, G. Baldi, S. Sicardi, Heat transfer in packed bed reactors with one phase flow, Chem. Eng. Commun. 4 (1980) 361–380, https://doi.org/10.1080/00986448008935916.
[44] D. Schlereth, O. Hinrichsen, Chemical engineering research and design a fixed-bed reactor modeling study on the methanation of CO_2, Chem. Eng. Res. Des. 92 (2013) 702–712, https://doi.org/10.1016/j.cherd.2013.11.014.